RSC Advances

ROYAL SOCIETY OF CHEMISTRY

www.rsc.org/advances

Synthesis, Structure and Luminescence Properties of New Blue-Green-Emitting Garnet-Type $Ca_3Zr_2SiGa_2O_{12}$: Ce^{3+} Phosphor for Near-UV Pumped White-LEDs

Jiyou Zhong[a, b], Weidong Zhuang [a, *], Xianran Xing[b], Ronghui Liu[a], Yanfeng Li[a], Yaling Zheng[a,b], Yunsheng Hu[a] and Huibing Xu [a]

[a] *National Engineering Research Center for Rare Earth Materials, General Research Institute for Nonferrous Metals, and Grirem Advanced Materials Co., Ltd., Beijing 100088, PR China*

[b] *Department of Physical Chemistry, University of Science & Technology Beijing, Beijing 100083, PR China*

**Corresponding authors:*

Weidong Zhuang. E-mail:wdzhuang@126.com. Tel: 86-10-82241333. Fax: 86-10-62355405

Abstract: A new blue-green-emitting phosphor $Ca_3Zr_2SiGa_2O_{12}:Ce^{3+}$ has been synthesized by conventional high temperature solid-state reaction method from the viewpoint of exploring new luminescent materials for white light-emitting diodes. The crystal structure of $Ca_3Zr_2SiGa_2O_{12}$ was investigated by the powder X-ray diffraction refinement and verified to be garnet-type with $Ia\bar{3}d$ space group and lattice constant $a=b=c$=12.5730(7) Å. The luminescence properties, concentration quenching, fluorescence lifetime, thermal quenching, quantum efficiency, chromaticity coordinates and related mechanisms of $Ca_3Zr_2SiGa_2O_{12}:Ce^{3+}$ phosphor was investigated in detail. The optimized phosphor shows two main broad excitation bands with peaks at 330 nm and 400 nm, respectively, in the region of 300-450 nm, and exhibits intense blue-green emission with peak wavelength at 478 nm under 400 nm excitation. The above results indicated that the phosphor can be effectively excited by near ultraviolet light and may have the potential applications as a near UV-convertible phosphor for white light-emitting diodes.

1. Introduction

Due to their high energy saving, long lifetime and environmental friendliness compared to traditional light sources such as incandescent and fluorescent lamps, white light-emitting diodes (w-LEDs) have attracted lots of attentions in solid-state lighting area [1-3]. Currently, the widely used w-LEDs fabricated by combining blue LED chip with $Y_3Al_5O_{12}:Ce^{3+}$ (YAG: Ce^{3+}) yellow-emitting phosphor is facing problems of high color temperature (CCT) and poor color rendition (RI) [4, 5], so that a near ultraviolet (*n*-UV, 380-420 nm) LED chip coated with tricolor phosphors was introduced, which can provide superior color uniformity with a high color rendering index and high quality white light [6, 7]. And the white light obtained by this approach is becoming more and more popular with a rising market occupation. However, the excitation energy levels of the traditional UV phosphors for fluorescent lamp are too high for *n*-UV LEDs. Therefore, to explore new phosphor materials, which meet the demand of *n*-UV excitation, are desired in the development process of w-LEDs.

It is well-known that the Ce^{3+}-activated garnet-type phosphors, typically, YAG: Ce^{3+} and $Ca_3Sc_2Si_3O_{12}$: Ce^{3+} phosphors, play important roles in presently commercial phosphors market, which implies high efficiency and excellent stability in these rigid garnet structure materials [8, 9]. However, both of the above mentioned garnet materials are suitable for blue light excitation, but have a weak excitation in *n*-UV region. Generally, the excitation and emission bands of f-d transition allowed Ce^{3+} ion is tunable depending on crystal field by composition adjustment, and a basis of an empirical rule for garnet phosphor is formed, that is, according to which substitutions of the dodecahedral ion by larger ions red shift the Ce^{3+} emission and substitutions of the octahedral ion by larger ions blue shift it [10]. And this provides insight to develop a new and

efficient garnet-type phosphor for *n*-UV LEDs.

Generally, there is three ways to find a new matrix material for phosphor. One is completely new finding in composition, phase and structure according to phase diagram analysis, such as $Ba_3Si_6O_{12}N_2$ [11], and this always means fortuitous. Another is searching for the reported compounds in the database, and this way is widely used over the past few decades, such as the development of $Sr_2Si_5N_8$: Eu^{2+}, Sr_3AlO_4F: Ce^{3+}, etc. [12-16], phosphors. However, the popular way in nowadays is substitutions, including single element equivalent substitution and multi elements substitution like Mg^{2+}-Si^{4+} replacing Al^{3+}-Al^{3+} [17-19], Si^{4+}-N^{3-} replacing Al^{3+}-O^{2-} [20, 21], Na^{+}-Sc^{3+} replacing Ca^{2+}-Mg^{2+} [22, 23], etc., typically, the $Ca_2Sc_2Si_3O_{12}$: Ce^{3+} is derived from Si^{4+} replacing Ge^{4+} in $Ca_2Sc_2Ge_3O_{12}$:Ce^{3+} [24]. In this work, we have tried to search a new matrix in the existing inorganic crystal structure database, which has the garnet-type structure and not been reported as phosphor matrix. And a matrix with formula $Ca_3Sn_2SiGa_2O_{12}$ [25] caused our attention, because the dodecahedral Ca^{2+} site is expected to introduce Ce^{3+} ion, however, the Sn^{4+} ion trends to be reduced to low valence states in reducing atmosphere. So, we intended to totally replace Sn^{4+} with Zr^{4+}, which has relatively stable valence state in reduction process. Thus a completely new compound with formula $Ca_3Zr_2SiGa_2O_{12}$ has been proposed and synthesized. To verify the garnet structure, the powder X-ray diffraction refinement was performed. The luminescence properties, concentration quenching, fluorescence lifetime, thermal quenching, quantum efficiency, chromaticity coordinates and related mechanisms of Ce^{3+} doped $Ca_3Zr_2SiGa_2O_{12}$ phosphor was investigated in detail.

2. Experimental

2.1. Materials and synthesis

The garnets with formula $Ca_{3-3x/2}Zr_2SiGa_2O_{12}:xCe^{3+}$ (x=0~0.16) were synthesized by high-temperature solid-state reaction method. The starting materials $CaCO_3$ (Aldrich, 99.95%), Ga_2O_3 (Aldrich, 99.9%), ZrO_2 (Aldrich, 99.9%), SiO_2 (Aldrich, 99.99%) and CeO_2 (Aldrich, 99.995%) were weighed out according to the stoichiometric ratio. The mixed powder was grounded evenly in an agate mortar, and then the homogeneous mixtures were put in an alumina crucible and continually fired at 1400 °C in a reducing atmosphere (CO) for 5 h.

2.2. Characterization methods

The crystal structure determination of the as-prepared $Ca_3Zr_2SiGa_2O_{12}$ garnet were performed by an X-ray diffraction (XRD) analysis using an X-ray powder diffractometer (Rigaku, Japan) with Co-Ka radiation (λ=0.178892 nm). The data were collected cover a 2θ range from 10° to 100° at intervals of 0.02° with a count time of 5 s per step. The structural parameters of $Ca_3Zr_2SiGa_2O_{12}$ garnet was refined by the Rietveld method using the *Fullprof software* [26]. The photoluminescence spectra and thermal quenching were measured by a spectrofluorometer (Fluoromax-4, Edison, U.S.A.), which are mainly composed of a Xe high-pressure arc lamp, a photomultiplier tube and a heating apparatus. Quantum efficiency was measured using the integrating sphere on the QE-2100 quantum yield measurement system (Otsuka Electronics Co., Ltd., Japan), and a Xe lamp was used as an excitation source and white $BaSO_4$ powder as a reference. The decay curves of Ce^{3+} lifetime values with various concentrations were measured by a TemPro-01 time-resolved fluorescence spectrofluorometer (U.S.A.).

3. Results and discussion

3.1. Phase and crystal structure analysis

The $Ca_3Zr_2SiGa_2O_{12}$ host and a series of Ce^{3+} doped $Ca_3Zr_2SiGa_2O_{12}$ phosphors were prepared

by a high temperature solid-state reaction method. Figure 1 presents the powder XRD patterns for $Ca_{3-3x/2}Zr_2SiGa_2O_{12}:xCe^{3+}$ (x=0~0.16) compared with standard pattern of inorganic crystal structure database (ICSD no. 73815) for $Ca_3Sn_2SiGa_2O_{12}$. The diffraction patterns of these samples can be indexed to the $Ia\bar{3}d$ space group of the cubic system and no diffraction peaks of impurities are detected in the experimental range, which indicated high purity of the phases and the doped Ce^{3+} ions did not generate any impurity or induce significant changes in the host structure. In order to verify the garnet-type crystal structure and obtain detailed structural information of these compounds, the Rietveld structural refinements of powder diffraction pattern for $Ca_3Zr_2SiGa_2O_{12}$ was performed (as shown in Figure 2) by using the $Ca_3Sn_2SiGa_2O_{12}$ garnet compound as starting model. The final refined unit cell parameters, atoms coordinates and residual factors are summarized in Table 1. The as-obtained goodness of fit parameters and cell parameters are $\chi^2 = 2.08$, $R_p = 6.80\%$, and $a = b = c = 12.5730(7)$ Å for $Ca_3Zr_2SiGa_2O_{12}$, which can ensure the garnet structure. Basing on these results, the crystal structure of $Ca_3Zr_2SiGa_2O_{12}$ was depicted in Figure 3a, which is constructed with $[ZrO_6]$ octahedrons, $[Ga/SiO_4]$ tetrahedrons and dodecahedral coordinated Ca^{2+} occupying interstitial position. As presented in Figure 3b, the $[CaO_8]$ dodecahedron connects with neighboring $[CaO_8]$ dodecahedron or $[ZrO_6]$ octahedron by sharing edges, while the $[Ga/SiO_4]$ tetrahedron connects with $[ZrO_6]$ octahedron or $[Ga/SiO_4]$ tetrahedron by sharing O^{2-} points. And those connections form the three dimensional network of the typical garnet structure.

3.2. Luminescence properties

The photoluminescence excitation (PLE) and emission (PL) spectrum of a selected $Ca_{3-3x/2}Zr_2SiGa_2O_{12}:xCe^{3+}$ (x=0.04) sample is shown in Figure 4. The PLE spectrum (monitored at

478 nm) contains two main broad excitation bands with excitation peaks at about 330 and 400 nm, respectively, which are attributed to the crystal field splitting of Ce^{3+} 5d states under D_2 symmetry constraints[19, 27]. Obviously, the position of the lowest Ce^{3+} $4f^1$-$5d_1$ absorption transition in $Ca_3Zr_2SiGa_2O_{12}$: Ce^{3+} is at a much higher energy level than that of common garnet-type phosphors, such as YAG: Ce^{3+}, CSS: Ce^{3+}, etc., which indicated a much weaker crystal field strength in this garnet phosphor. The reason mainly ascribes to the large ionic radii Zr^{4+} ion occupying octahedral site, which dramatically expands the lattice parameters and produces a relaxed environment for Ce^{3+} ion [28, 29]. What's more, the broad excitation band from 380 to 420 nm with peak at 400nm is a good fit for the excitation of the *n*-UV LED chip. Under *n*-UV light (λ_{ex} = 400 nm) excitation, the PL spectrum exhibits an asymmetric blue-green emission band ranging from 430 to 600 nm with an emission peak at about 478 nm. The formation of asymmetric emission spectrum may not only due to the transition of the Ce^{3+} ions from the 5d excited state to the $^2F_{5/2}$ and $^2F_{7/2}$ two ground states, but also the Ce^{3+} ions occupying more than one differentiated Ca^{2+} ions site in the lattice since the Ga^{3+} and Si^{4+} are randomly distributed on the 24d site, the second-sphere around Ce^{3+} ion is possible to have different Si^{4+}/Ga^{3+} ratio and this can affect the O^{2-} ions directly connected to Ce^{3+} ion in the first-sphere [30].

Figure 5 presents the PL spectra of $Ca_{3-3x/2}Zr_2SiGa_2O_{12}$:x$Ce^{3+}$ (x=0.02~0.16) under 400 nm excitation measured at room temperature. It is observed that the emission intensity of Ce^{3+} ion firstly increases until reaching a maximum at x = 0.04, and then gradually decreases with the increase of Ce^{3+} concentration (Figure 5, inset). Thus the critical Ce^{3+} concentration was optimized to be x=0.04, beyond which the possibility of nonradiative energy transfer between Ce^{3+} ions increases and leading to concentration quenching. The critical distance R_c of energy transfer

between Ce^{3+} ions in $Ca_3Zr_2SiGa_2O_{12}$: Ce^{3+} can be calculated according to the following equation [31]:

$$R_c \approx 2[\frac{3V}{4\pi x_c N}]^{1/3} \quad (1)$$

Where V is the volume of the crystallographic unit cell, x_c is the critical concentration and N is the number of lattice sites in the unit cell that can be occupied by the activator ion. In the present case, the values V=1987.57(7) Å^3, N=24, and x_c=0.04, so the critical distance R_c is calculated to be 16 Å. Generally, energy transfer between different Ce^{3+} ions can occur via radiation reabsorption, exchange or multipolar interactions [32]. According to the calculated critical distance, it can be inferred that the mechanism of exchange interaction plays no role in energy transfer between Ce^{3+} ions in the $Ca_3Zr_2SiGa_2O_{12}$: Ce^{3+} since the exchange interaction requires a forbidden transition and a typical critical distance of 5 Å [33]. Therefore, it can be inferred if the energy transfer occurs only by electric multipolar interaction, the interaction type between Ce^{3+} ions can be determined via the following equation according to Dexter's theory [34]:

$$I / x = k[1 + \beta(x)^{\theta/3}]^{-1} \quad (2)$$

here in this equation, I is the emission intensity corresponding to activator concentration x, k and β are constants for the same excitation condition for a certain host crystal, and θ is a function of the multipole-multipole interaction. θ=6, 8 and 10 corresponds to dipole-dipole (d-d), dipole-quadrupole (d-q), and quadrupole-quadrupole (q-q) interactions, respectively. By linear fitting the relationship of lg(I/x) vs lg(x) with a slope of -1.57 (as shown in Figure 6), the calculated θ=4.7, which is relative close to 6, suggests that dipole-quadrupole (d-q), and quadrupole-quadrupole (q-q) interactions also play no role in the process of Ce^{3+} concentration quenching in the present $Ca_3Zr_2SiGa_2O_{12}$: Ce^{3+} phosphor. As there is a not negligible overlap

between the excitation and emission bands, the reabsorption effect should be taken into consideration in the energy transfer process. Therefore, the possible energy transfer mechanism for concentration quenching mainly ascribes to dipole-dipole interaction and radiation reabsorption.

It is also found that the PL spectrum markedly shifts to longer wavelengths (red shift) with the increase of Ce^{3+} concentration (Figure 5, inset). The emission peak shifts from 469 to 494 nm having a wavelength offset approximate 25 nm with various Ce^{3+} concentrations (x=0.005~0.16). And this kind of red-shift is mainly ascribed to larger ions replacing smaller ions in dodecahedral sites of garnet-type phosphor [6, 35, 36], because with the increasing concentration of larger Ce^{3+} ion ($r(Ce^{3+})$=1.14 Å, CN=8) substituting Ca^{2+} ion ($r(Ce^{3+})$=1.12 Å, CN=8) in dodecahedral site, it is possible to make more compression on Ce^{3+}-O^{2-} bond in the rigid garnet structure, and the distance between Ce^{3+} and O^{2-} becomes shorter, the crystal field strength increases, and resulting in emission wavelength red-shift [10, 37]. On the other hand, the probability of the energy transfer from Ce^{3+} ions at higher levels of 5d to those at lower levels of 5d was promoted with the increase of Ce^{3+} concentration, thus the emission at high energy decreases and the emission at low energy increases, which also leads to red shifts in the emission spectrum [19]. Both of the above mentioned factors for spectrum red-shift cannot be neglected in these garnet-type phosphors.

Figure 7 presents the fluorescence decay curves of $Ca_{3-3x/2}Zr_2SiGa_2O_{12}:xCe^{3+}$ (x=0.02~0.12) phosphors under 389 nm excitation and monitored at 480 nm. Generally, the value of lifetime can be calculated by fitting first-order exponential decay function, and with this method, the decay times were determined to be 28.4, 25.2, 23.6, 22.5 and 21.9 ns for $Ca_{3-3x/2}Zr_2SiGa_2O_{12}:xCe^{3+}$ phosphors with varying Ce^{3+} doped concentrations, respectively, which are short enough for potential applications in w-LEDs. Obviously, the decay time trends to decrease gradually with

further increasing Ce^{3+} concentration, which indicates that the nonradiative and self-absorption are gradually enhanced [33]. It is also found that the relationship of ln[I_t] vs t gradually deviates from linear function with increasing of Ce^{3+} concentration, which reveals that more and more Ce^{3+} ions occupying the differentiated Ca^{2+} ions sites.

The thermal quenching property is one of the key application criterions for phosphors. Figure 8 presents the temperature dependent emission spectra of the optimized $Ca_{2.94}Zr_2SiGa_2O_{12}$:$0.04Ce^{3+}$ phosphor under excitation at 400 nm and the inset shows the relative emission intensities as a function of temperature. It is revealed that the relative PL intensity decreases with the increase of temperature, and still 73% of the initial emission intensity (at room temperature) remains when the temperature was raised up to 100 °C. Generally, the thermal quenching process is explained as increased nonradiative relaxation probability induced by enhanced phonon-electron interaction with the increase of temperature. The nonradiative relaxation process occurs when the excited electron cross the crossing point between the ground and excited states. The energy barrier for thermal quenching is defined as activation energy for thermal quenching, which can be calculated by Arrhenius equation [33, 38]:

$$I_T = \frac{I_0}{1 + c\exp(\frac{-\Delta E}{kT})} \quad (2)$$

where I_0 is the initial emission intensity, I_T is the intensity at different temperatures, ΔE is activation energy of thermal quenching, c is a constant for a certain host, and k is the Boltzmann constant (8.629×10^{-5} eV). By linear fitting the relationship of ln[(I_0/I_T)-1] vs 10000/T for the $Ca_{2.94}Zr_2SiGa_2O_{12}$:$0.04Ce^{3+}$ phosphor with a slope of -0.39 (as shown in Figure 9), the activation energy was calculated to be 0.39 eV. Moreover, with the increase of the temperature, the shape of the emission spectra does not show significant change and the position of emission peak shows a

negligible red-shift with a wavelength offset only about 2 nm, which indicates excellent color stability of this phosphor under different temperatures. Furthermore, the CIE chromaticity coordinates for $Ca_3Zr_2SiGa_2O_{12}:xCe^{3+}$ (x=0.02~0.16) phosphors excited at 400 nm were determined and the CIE coordinates are calculated to be ranged from (0.171, 0.248) to (0.235, 0.381) (depicted in Figure 10). A digital photo of the $Ca_{2.94}Zr_2SiGa_2O_{12}:0.04Ce^{3+}$ phosphor under 254 nm UV lamp is shown in the inset of Figure 10, revealing an intense blue-green light emission. Finally, the internal quantum efficiency of the optimized sample $Ca_{2.94}Zr_2SiGa_2O_{12}:0.04Ce^{3+}$ phosphor was measured to be 42.7% at room temperature. And this is expected to be further improved by synthesis and composition optimization, especially, making further substitutions, such as Al^{3+} replacing Ga^{3+}, which is conducive to reduction of inevitable thermal ionization [39, 40].

4. Conclusions

In summary, a new blue-green garnet-type phosphor $Ca_3Zr_2SiGa_2O_{12}:Ce^{3+}$ has been successfully synthesized by conventional high temperature solid-state reaction method. The garnet structure was further confirmed by powder X-ray diffraction refinement. The $Ca_3Zr_2SiGa_2O_{12}:Ce^{3+}$ phosphor shows two main broad excitation bands with peaks at 330 nm and 400 nm in the region of 300-450 nm, and exhibits intense blue-green emission with peak wavelength about at 478 nm under 400 nm near ultraviolet light excitation. The optimal Ce^{3+} doping concentration was x=0.04 with an internal quantum efficiency of about 42.7%. The value of the critical distance is 16 Å, and the corresponding concentration quenching mechanism is considered to be the dipole-dipole interaction and radiation reabsorption. The temperature dependent luminescence behaviors suggested a moderate thermal quenching property of this phosphor. The above results indicated that the phosphor can be effectively excited by *n*-UV light and may have the potential applications

as an *n*-UV-convertible phosphor for w-LEDs.

Acknowledgments

This present work was financially supported by the National Basic Research Program of China (2014CB643801), and the National Natural Science Foundation of China (51302016).

References

1 E. F. Schubert and J. K. Kim, *Science*., 2005, **308**, 1274.

2 S. Nakamura, T. Mukai and M. Senoh, *Appl. Phys. Lett*., 1994, **64**, 1687.

3 S. Pimputkar, S J. S. peck, S. P. DenBaars and S. Nakamura, *Nature Photon*., 2009, **3**, 180.

4 Y. Chen, M. Gong, G. Wang and Q. Su, *Appl. Phys. Lett*., 2007, **91**, 1117.

5 H. S. Jang, W. B. Im, D. C. Lee, D. Y. Jeon, and S. S. Kim, *J. Lumin.*, 2007, **126**, 371.

6 V. Bachmann, C. Ronda, and A. Meijerink, *Chem. Mater.*, 2009, **21**, 2077.

7 Z. Xia and R. S. Liu, *J. Phys. Chem. C.*, 2012, **116**, 15604.

8 N. C. George, A. J. Pell, G. Dantelle, K. Page, A. Llobet, M. Balasubramanian, G. Pintacuda, B. F. Chmelka and R. Seshadri, *Chem.Mater.*, 2013, **25**, 3979.

9 J. Brgoch, S. P. DenBaars and R. Seshadri, *J. Phys. Chem. C.*, 2013, **117**, 17955.

10 A. B. Munoz-García and L. Seijo, *J. Phys. Chem. A.*, 2011, **115**, 815.

11 M. Mikami, H. Watanabe, K. Uheda, S. Shimooka, Y. Shimomura, T. Kurushima and N. Kijima. IOP Conference Series: *Mat. Sci. Eng.*, 2009, **1**, 012002.

12 Y. Q. Li, J. E. J. Van Steen, J. W. H. Van Krevel, G. Botty, A.C.A. Delsing, F.J. DiSalvo, G. de With and H.T. Hintzen. *J. Alloys Compounds.*, 2006, **417**, 273.

13 W. B. Im, S. Brinkley, J. Hu, A. Mikhailovsky, S. P. DenBaars and R. Seshadri, *Chem. Mater.*, 2010, **22**, 2842.

14 J. Zhong, W. Zhuang, X. Xing, R. Liu, G. Chen, Y. Liu and L. Chen, *Mater. Lett.*, 2014, **131**, 248.

15 K. W. Huang, W. T. Chen, C. I. Chu, S. F. Hu, H. S. Sheu, B. M. Cheng, J. M. Chen and R. S. Liu, *Chem. Mater.*, 2012, **24**, 2220.

16 J. Zhou, Z. Xia, M. Yang and K. Shen, *J. Mater. Chem.*, 2012, **22**, 21935.

17 M. Shang, J. Fan, H. Lian, Y. Zhang, D. Geng and J. Lin, *Inorg. Chem.*, 2014, **53**, 7748.

18 Y. Shi, G. Zhu, M. Mikami, Y. Shimomura and Y. Wang, *Dalton Trans.*, 2015, **44**, 1775.

19 A. A. Setlur, W. J. Heward, Y. Gao, A. M. Srivastava, R. G. Chandran and M. V. Shankar, *Chem. Mater.* , 2006, **18**, 3314-3322.

20 A. A. Setlur, W. J. Heward, M. E. Hannah and U. Happek, *Chem. Mater.*, 2008, **20**, 6277.

21 W.T. Chen, H.S. Sheu, R.S. Liu and J. P. Attfield, *J. Am. Chem. Soc.*, 2012, **134**, 8022

22 Z. Xia, Y. Zhang, M. S. Molokeev and V. V. Atuchin, *J. Phys. Chem. C*, 2013, **117**, 20847.

23 S. Ray, Y. C. Fang and T. M. Chen, *RSC Adv.*, 2013, **3**, 16387

24 Y. Shimomura, T. Honma, M. Shigeiwa, T. Akai, K. Okamoto, and N. Kijima, *J. Electrochem. Soc.*, **2007**, 154, J35.

25 A. Rulmont, P. Tarte, B. Cartié, J. Choisnet, *J. Solid State Chem.*, 1993, **104**, 165.

26 16 J. Rodríguez-Carvajal, *Commission on powder diffraction (IUCr). Newsletter*, 2001, **26**, 12.

27. L. Seijo, Z. Barandiarán, *Phys. Chem. Chem. Phys.*, 2014, **16**, 3830.

28 X. Wang and Y. Wang, *J. Phys. Chem. C*, 2015, **119**, 16208.

29 X. Gong, J. Huang, Y. Chen, Y. Lin, Z. Luo and Y. Huang, *Inorg. Chem.*, 2014, **53**, 6607.

30 W. Y. Huang, F. Yoshimura, K. Ueda, W. K. Pang, B. J. Su, L. Y. Jang, C. Y. Chiang, W. Zhou, N. H. Duy and R. S. Liu, *Inorg. Chem.*, 2014, **53**, 12822.

31 G. Blasse, *J. Solid State Chem.*, 1986, **62**, 207-211.

32 J. Zhong, W. Zhuang, X. Xing, R. Liu, Y. Li, Y. Liu and Y. Hu, *J. Phys. Chem. C*, 2015, **119**, 5562.

33 Z. Xia, R. S. Liu, K. W. Huang and V. Drozd, *J. Mater. Chem.,* 2012, **22**, 15183.

34 D. L. Dexter, *J. Chem. Phys.* , 1953, **21**, 836.

35 Q. Shao, H. Li, Y. Dong, J. Jiang, C. Liang and J. He, *J. Alloys Compounds.* , 2010, **498**, 199.

36 C. C. Chiang, M. S. Tsai and M. H. Hon, *J. Alloys Compounds.* , 2007,**431**, 298.

37 X. Chen, Z. Xia and Q. Liu, *Dalton Trans.*, 2014, **43**, 13370

38 C. H. Huang and T. M. Chen, *Inorg. Chem.* , 2011, **50**, 5725.

39 J. Ueda, K. Aishima and S. Tanabe, *Opt. Mater.* , 2013, **35**, 1952.

40 J. Ueda, P. Dorenbos, A. J. J. Bos, A. Meijerink and S. Tanabe, *J. Phys. Chem. C*, 2015, **119**, 25003

Table 1. Results of Structure Refinement of $Ca_3Zr_2SiGa_2O_{12}$

formula			$Ca_3Zr_2SiGa_2O_{12}$			
symmetry			cubic			
space group			$Ia\bar{3}d$			
$a = b = c$ (Å)			12.5730(7)			
α =β= γ (deg)			90			
V (Å^3)			1987.57(7)			
Z			8			
R_p (%)			6.80			
R_{wp} (%)			9.81			
χ^2			2.08			
atom	site	x	y	z	occu.	Biso
Ca	24c	0.12500	0.00000	0.25000	0.25000	0.10906
Zr	16a	0.00000	0.00000	0.00000	0.16667	0.09194
Si	24d	0.37500	0.00000	0.25000	0.08333	0.11682
Ga	24d	0.37500	0.00000	0.25000	0.16667	0.11682
O	96h	0.96585	0.05151	0.15489	1.00000	0.12928

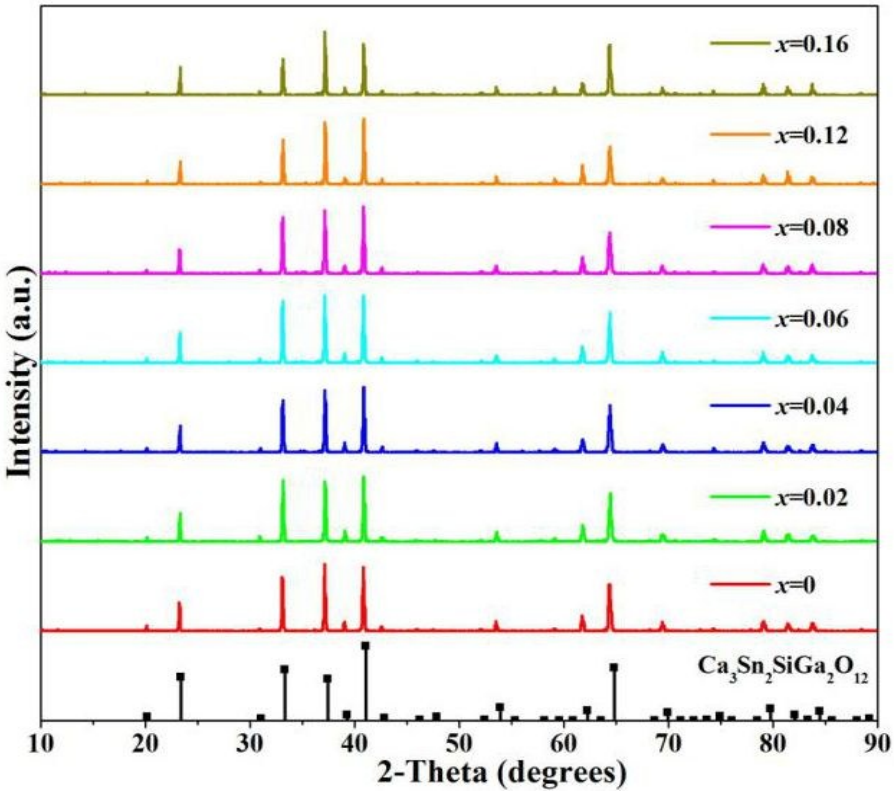

Figure 1. Powder XRD patterns of as-prepared $Ca_{3-3x/2}Zr_2SiGa_2O_{12}$:$xCe^{3+}$ (x=0~0.16) samples and ICSD card (no. 73815) of $Ca_3Sn_2SiGa_2O_{12}$ compound is also given for comparison.

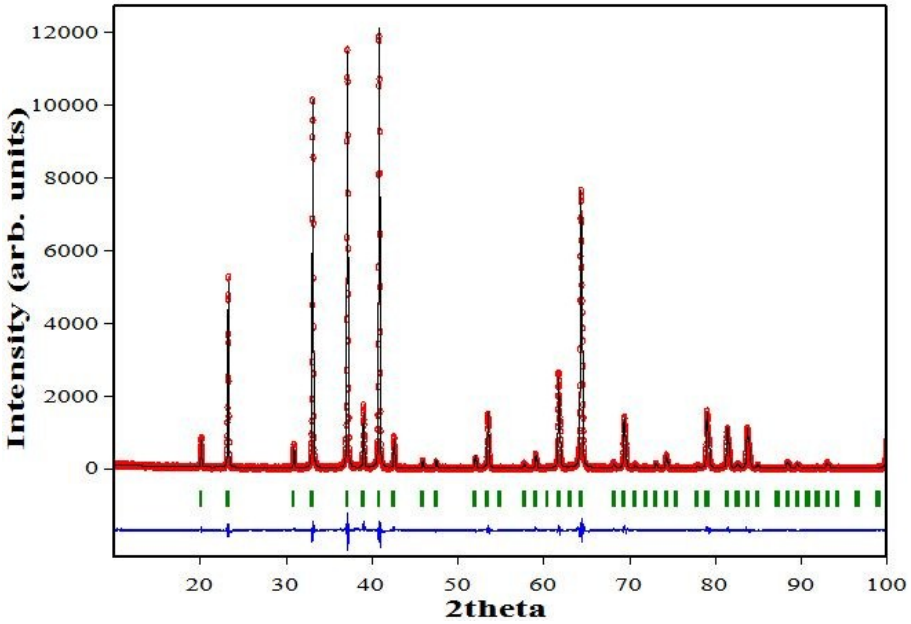

Figure 2. Powder XRD pattern (red circles) of $Ca_3Zr_2SiGa_2O_{12}$ with its corresponding Rietveld refinement (black solid line) and residuals (blue line in the bottom).

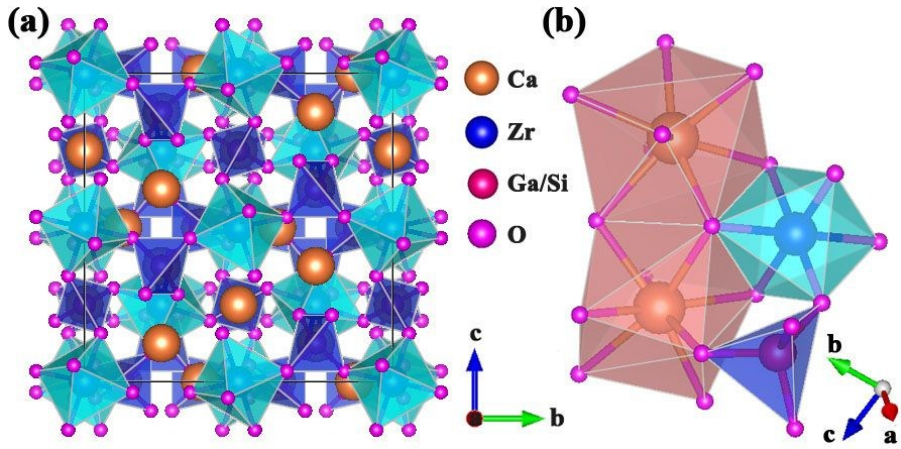

Figure 3. (a) Crystal structure of $Ca_3Zr_2SiGa_2O_{12}$, and (b) the connections between polyhedrons.

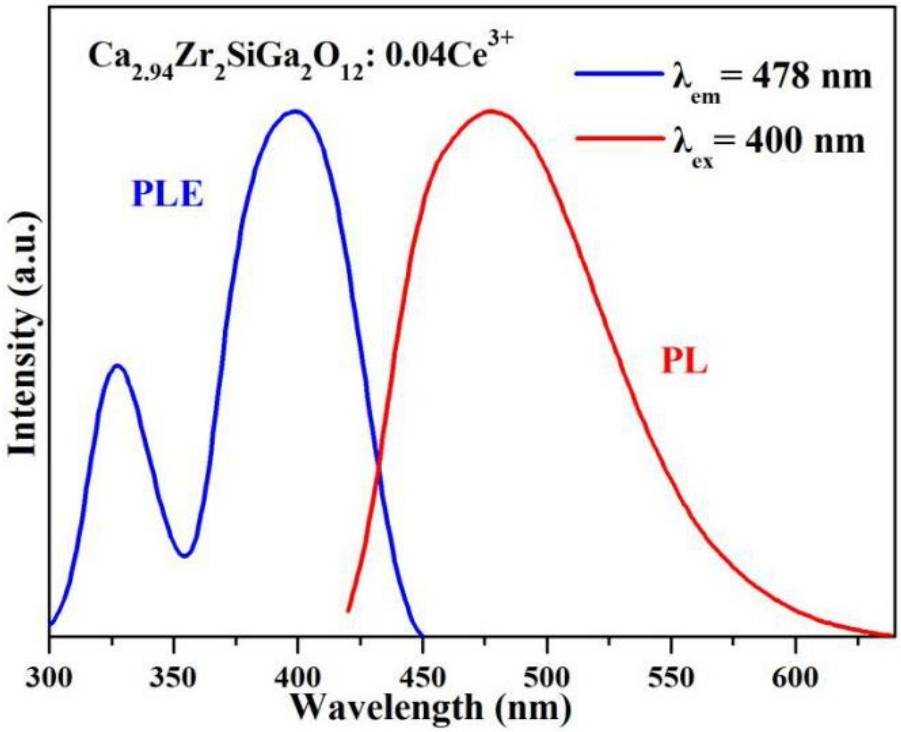

Figure 4. PLE and PL spectra of $Ca_{2.94}Zr_2SiGa_2O_{12}$:0.04$Ce^{3+}$ phosphor.

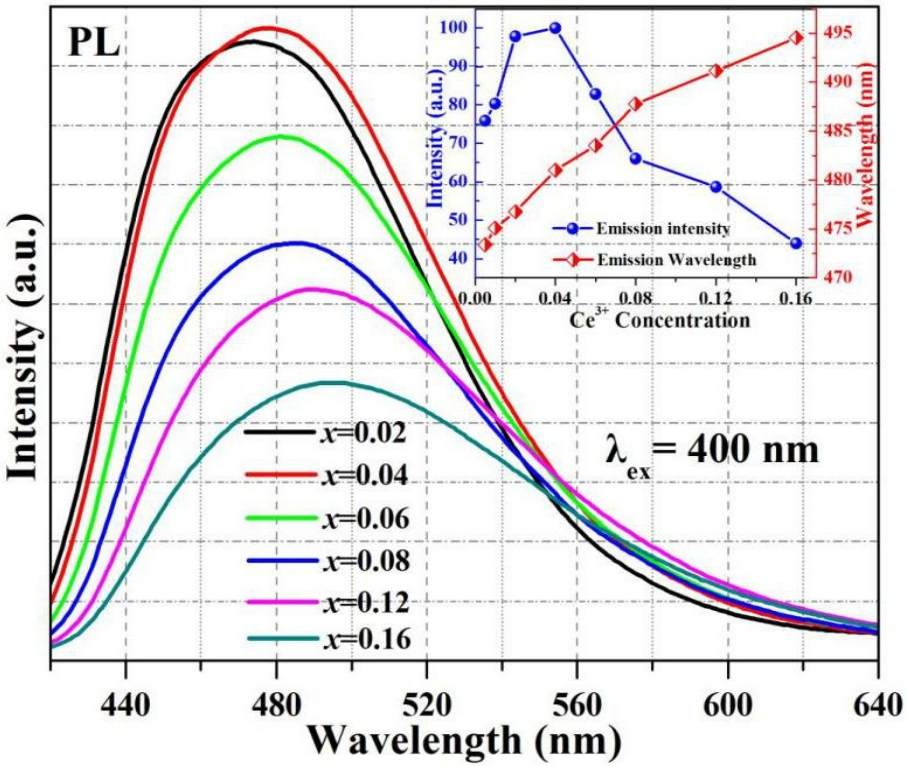

Figure 5. PL (λ_{ex}=400 nm) spectra of $Ca_{3-3x/2}Zr_2SiGa_2O_{12}$:x$Ce^{3+}$ with varying Ce^{3+} concentrations; inset shows the emission intensity and emission peak wavelength as a function of the Ce^{3+} content.

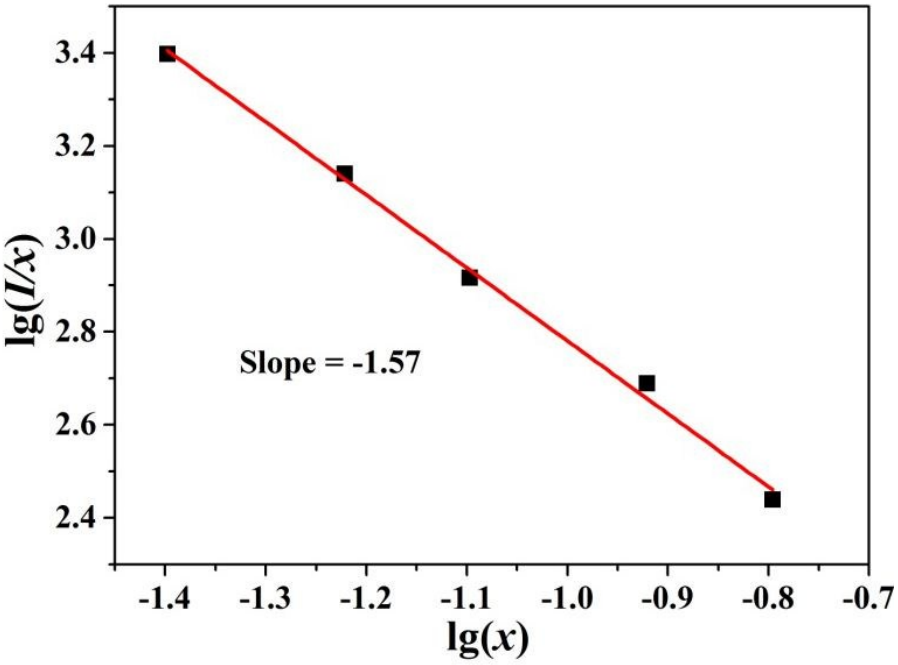

Figure 6. Linear fitting of the relationship of lg(I/x) vs lg(x).

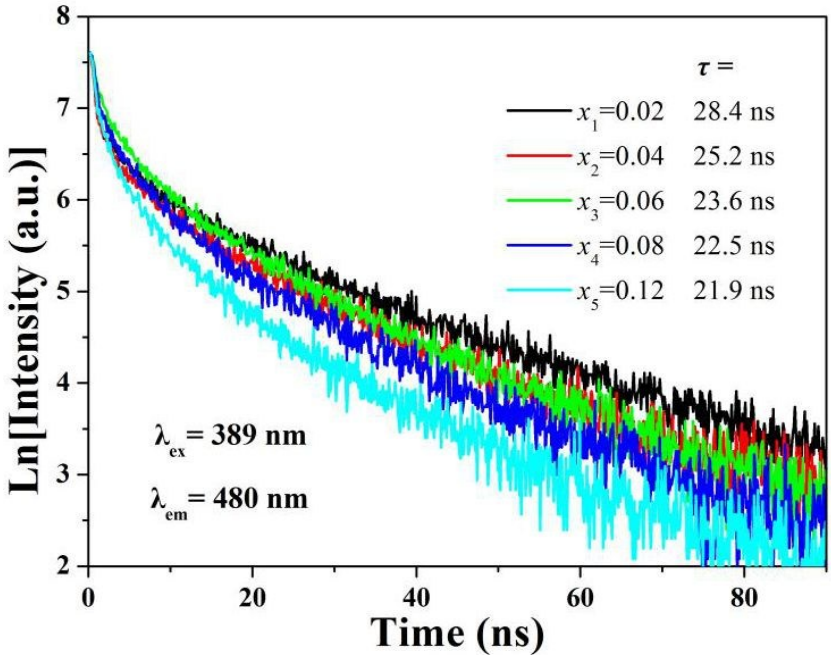

Figure 7. Decay curves and calculated lifetimes of $Ca_{3-3x/2}Zr_2SiGa_2O_{12}:xCe^{3+}$ with varying Ce^{3+} concentrations.

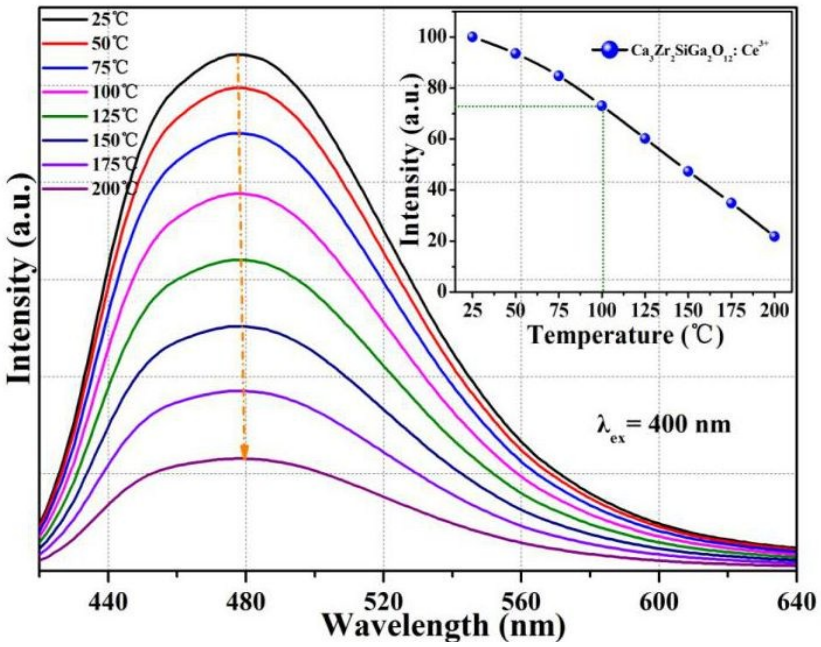

Figure 8. Temperature dependent emission spectra of $Ca_{2.94}Zr_2SiGa_2O_{12}$:0.04$Ce^{3+}$ phosphor under excitation at 400 nm, the inset shows the relative emission intensities as a function of temperature in the range of 25–200 °C.

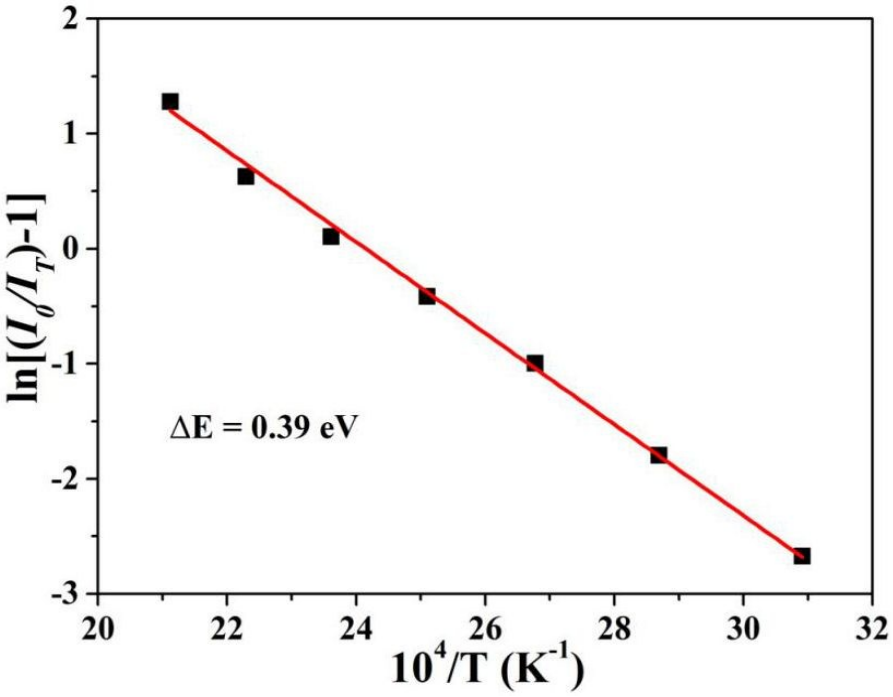

Figure 9. Arrhenius fitting of the emission intensity of $Ca_{2.94}Zr_2SiGa_2O_{12}$:0.04$Ce^{3+}$ phosphor and the calculated activation energy for thermal quenching.

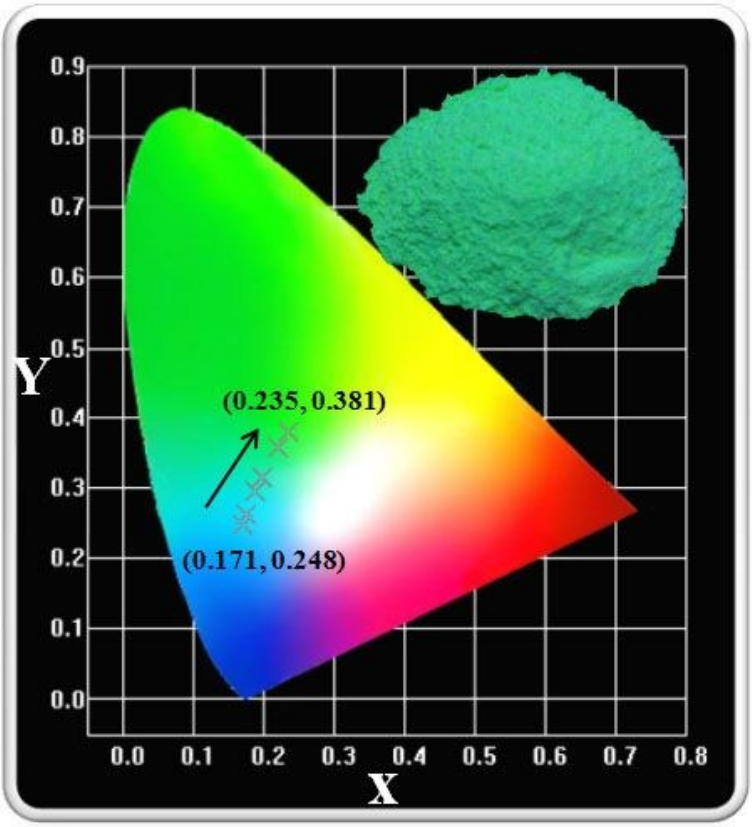

Figure 10. CIE coordinates of $Ca_{3-3x/2}Zr_2SiGa_2O_{12}:xCe^{3+}$ ($0.02 \leq x \leq 0.16$) phosphors with different Ce^{3+} concentrations under excitation at 400 nm, and a digital photo under 254 nm UV lamp of the optimized $Ca_{2.94}Zr_2SiGa_2O_{12}:0.04Ce^{3+}$ phosphor.

Synthesis, Structure and Luminescence Properties of New Blue-Green-Emitting Garnet-Type $Ca_3Zr_2SiGa_2O_{12}$: Ce^{3+} Phosphor for Near-UV Pumped White-LEDs

Jiyou Zhong[a, b], Weidong Zhuang [a, *], Xianran Xing[b], Ronghui Liu[a], Yanfeng Li[a], Yaling Zheng[a,b], Yunsheng Hu[a] and Huibing Xu [a]

[a] *National Engineering Research Center for Rare Earth Materials, General Research Institute for Nonferrous Metals, and Grirem Advanced Materials Co., Ltd., Beijing 100088, PR China*

[b] *Department of Physical Chemistry, University of Science & Technology Beijing, Beijing 100083, PR China*

**Corresponding authors:*

Weidong Zhuang. E-mail:wdzhuang@126.com. Tel: 86-10-82241333. Fax: 86-10-62355405

Graphical abstracts

A new blue-green-emitting garnet-type phosphor $Ca_3Zr_2SiGa_2O_{12}$:Ce^{3+} has been explored for *n*-UV pumped white light-emitting diodes.